Current Biology 25, 16–28, January 5, 2015 ©2015 Elsevier Ltd All rights reserved http://dx.doi.org/10.1016/j.cub.2014.10.071

Article

Neurobeachin Is Required Postsynaptically for Electrical and Chemical Synapse Formation

Adam C. Miller,[1,*] Lisa H. Voelker,[1,2] Arish N. Shah,[1] and Cecilia B. Moens[1]
[1]Division of Basic Sciences, Fred Hutchinson Cancer Research Center, 1100 Fairview Avenue N, Seattle, WA 98109, USA
[2]Molecular and Cellular Biology, University of Washington, 1959 NE Pacific Street, Seattle, WA 98195, USA

Summary

Background: Neural networks and their function are defined by synapses, which are adhesions specialized for intercellular communication that can be either chemical or electrical. At chemical synapses, transmission between neurons is mediated by neurotransmitters, whereas at electrical synapses, direct ionic and metabolic coupling occur via gap junctions between neurons. The molecular pathways required for electrical synaptogenesis are not well understood, and whether they share mechanisms of formation with chemical synapses is not clear.
Results: Here, using a forward genetic screen in zebrafish, we find that the autism-associated gene *neurobeachin* (*nbea*), which encodes a BEACH-domain-containing protein implicated in endomembrane trafficking, is required for both electrical and chemical synapse formation. Additionally, we find that *nbea* is dispensable for axonal formation and early dendritic outgrowth but is required to maintain dendritic complexity. These synaptic and morphological defects correlate with deficiencies in behavioral performance. Using chimeric animals in which individually identifiable neurons are either mutant or wild-type, we find that Nbea is necessary and sufficient autonomously in the postsynaptic neuron for both synapse formation and dendritic arborization.
Conclusions: Our data identify a surprising link between electrical and chemical synapse formation and show that Nbea acts as a critical regulator in the postsynaptic neuron for the coordination of dendritic morphology with synaptogenesis.

Introduction

Synaptogenesis proceeds through a prolonged process involving pre- and postsynaptic neuronal specification, dendritic and axonal guidance, the local choice of appropriate synaptic partners, and the trafficking and assembly synaptic machinery. These steps in synapse formation are coordinated with the morphological elaboration of neurons, leading to the proposal of the "synaptotrophic hypothesis," which posits that synaptogenesis supports and coordinates the development of neuronal morphology [1]. Chemical synapses rely on the precise apposition of synaptic vesicles (SVs) and exocytic machinery presynaptically with the postsynaptic neurotransmitter receptors and scaffolds that stabilize the synapse [2]. Importantly, neural circuits also contain electrical synapses, which are composed of gap junctions created by the coupling of hexamers of Connexins (Cxs) contributed from each side of the synapse [3]. These gap junctions create channels between the neurons allowing for direct ionic and metabolic communication [3]. Electrical synapses are used broadly during development but are also retained in adult sensory, central, and motor circuits [3–5]. Although progress has been made in elucidating mechanisms that regulate chemical synapse formation, the genes that underlie electrical synaptogenesis, and whether there are mechanistic commonalities in the formation of these two structurally dissimilar synapse types, are not known.

In a forward genetic screen in zebrafish, we identified a mutation in *neurobeachin* (*nbea*) as causing defects in the formation of electrical synapses. Nbea is a large (>320 kDa), multidomain protein that is highly conserved among vertebrates, and mutations have been identified in patients with nonsyndromic autism spectrum disorder [6–8]. It is expressed throughout the nervous system and localizes to tubulovesicular membranes near the *trans* side of Golgi and on pleomorphic vesicles in the cell body, dendrites, and axons [9–11]. Nbea belongs to the family of BEACH (Beige and Chediak-Higashi) domain-containing proteins, which have been implicated in cargo trafficking and endomembrane compartmentalization [6]. It contains many protein-protein interaction domains (tryptophan-aspartic [WD40] repeats, armadillo repeats), suggesting that it may function as a scaffold in the endomembrane system [6]. Although *nbea* mutant mice have no overt defects in endomembrane compartmentalization [11], they do have specific defects in synaptogenesis. *nbea* mutant mice lack movement and die shortly after birth due to asphyxia correlated with a lack of evoked SV release at neuromuscular junctions [9]. In the CNS, *nbea* mutants have defects in the function of the main excitatory and inhibitory synaptic types (glutamatergic and GABAergic synapses, respectively), and these deficits are correlated with morphological defects in the number of synaptic vesicles presynaptically and the size of the postsynaptic density [11–13]. Additionally, *nbea* mutants have reduced surface availability of glutamatergic and GABAergic receptors at synapses [11]. No role for Nbea in glycinergic synaptogenesis or electrical synapse formation has been described. Furthermore, whether Nbea controls synaptogenesis presynaptically, postsynaptically, or both, as well as whether it contributes to the elaboration of neuronal morphology, remains controversial [9, 11–13].

Here we show that Nbea is required for electrical and chemical synaptogenesis in vivo using the individually identifiable neurons and synapses of the zebrafish Mauthner escape circuit. We find that *nbea* mutants have defects in electrical and glycinergic chemical synaptogenesis, and that these defects correlate with deficiencies in the behavioral repertoires of mutant animals. These findings reveal an unexpected commonality in the pathways leading to the assembly of electrical and chemical synapses at the level of Nbea. Using chimeric animals in which identified neurons in the circuit are either mutant or wild-type, we find that *nbea* is necessary and sufficient autonomously in postsynaptic neurons for both electrical and chemical synapse formation. We find that *nbea* is also necessary and sufficient in the postsynaptic neuron for

*Correspondence: amiller@fhcrc.org

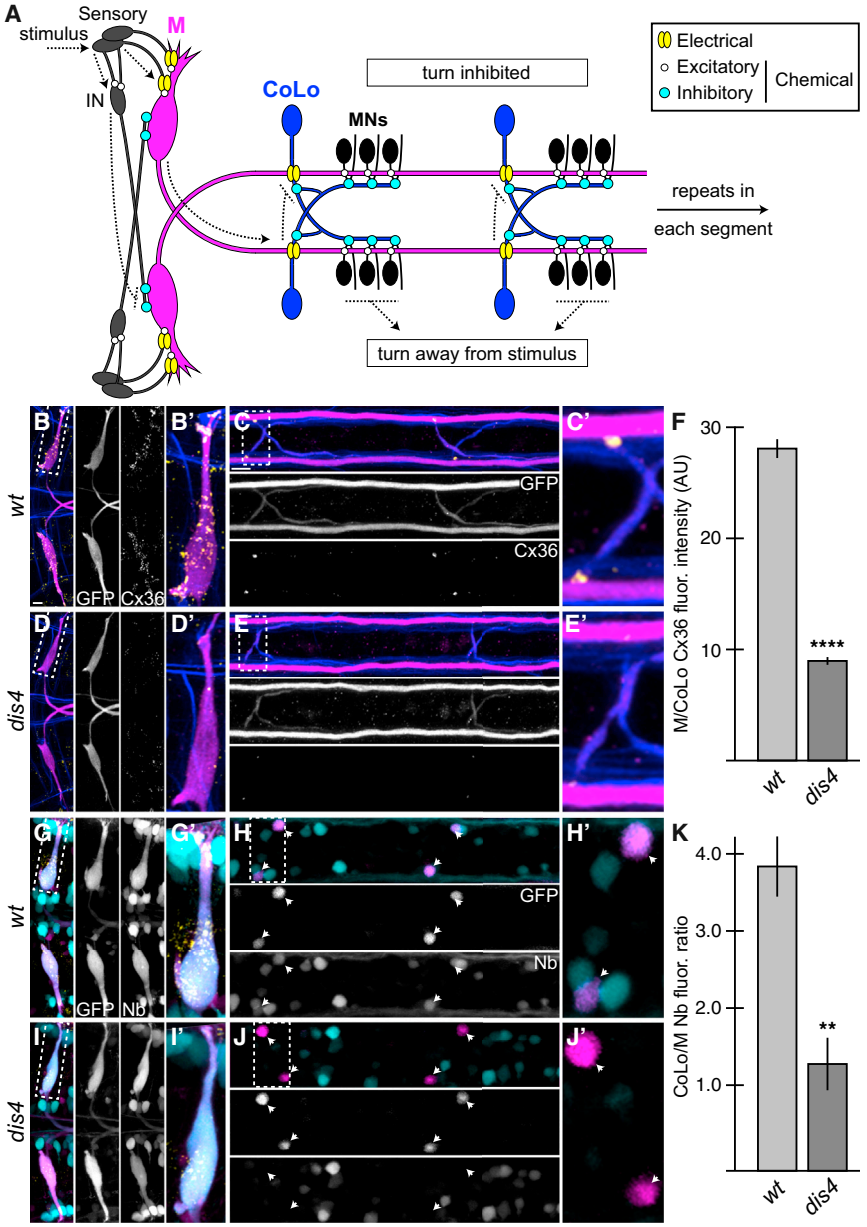

Figure 1. Electrical Synapses Are Disrupted in *dis4* Mutants

(A) Model of the Mauthner (M) circuit. Neurons, synapses, and behavioral output are depicted. Hindbrain and two spinal segments are shown. Dotted arrows depict flow of circuit activity given the indicated stimulus.

(B–E and G–J) In this and all subsequent figures, except where noted, images are dorsal views of hindbrain and two spinal cord segments from *M/CoLo:GFP* larvae at 5 days postfertilization (dpf). The (′) panels are zooms of the regions denoted by the dotted boxes. Hindbrain and spinal cord images are maximum-intensity projections of ~30 and ~10 μm, respectively. Anterior is to the left. Scale bar represents 10 μm. Larvae are stained for GFP (magenta) and Connexin36 (Cx36, yellow) in all panels, neurofilaments (RMO44, blue) in (B)–(E), and Neurobiotin (Nb, cyan) in (G)–(J). Individual GFP, Cx36, and Nb channels are shown in neighboring panels.

(B–E) The Cx36 staining found at M dendrites (B and B′) and M/CoLo synapses (C and C′) is reduced in *dis4* mutant animals (D and E).

(F) Quantitation of Cx36 at M/CoLo synapses in wild-type and *dis4* mutants.

(G–J) Electrical synapses are functionally defective in *dis4* mutants. Images show experiments in which M axons were filled with the gap-junction-permeable dye Nb from a caudal transection in the spinal cord. Spinal cord images are at the level of the CoLo cell bodies (arrowheads), which are dorsal to the synapses.

(G and H) Nb labels the M cell bodies and other caudally projecting neurons (G and G′) and passes through the Cx36 gap junctions to fill the CoLo cell bodies (H and H′, arrowheads). Other neurons are also labeled due to projections caudally into the lesion site.

(I and J) In *dis4* mutants, Nb labels M normally (I and I′); however, the amount passing into CoLos is diminished (J and J′, arrowheads).

(K) Quantitation of ratio of Nb in CoLo to M cell bodies in wild-type and *dis4* mutants.

Graphs in (F) and (K) represent data as mean ± SEM. **p < 0.01 and ****p < 0.0001 compared to control.

Associated experimental statistics are found in Table S2.

maintaining an elaborate dendritic arbor. Our data support the synaptotrophic hypothesis and suggest a model in which postsynaptic Nbea acts within the endomembrane system as coordinator of synaptogenesis and dendritic arborization.

Results

disconnect4 Mutants Have Defects in Electrical Synaptogenesis

To identify genes required for electrical synaptogenesis, we used the Mauthner (M) neural circuit of zebrafish (Figure 1A). The M circuit is well known for its role in a fast escape response to startling auditory and tactile stimuli and is wired to allow for very rapid turns away from threats [14]. The circuitry that accomplishes this is relatively simple: sensory neurons relay environmental stimuli via mixed electrical and chemical synapses onto the dendrites of the bilaterally paired M neurons located in the hindbrain. Each M sends a contralateral axon down the length of the spinal cord, where it makes segmentally repeated, en passant, excitatory chemical synapses with primary motor neurons (MNs) and separate electrical synapses with inhibitory commissural local (CoLo) interneurons. The CoLo interneurons function to suppress turns on the stimulus side by recrossing the spinal cord and inhibiting MNs and CoLos within the same segment. Additionally, sensory neurons in the hindbrain make excitatory chemical synapses with inhibitory interneurons that in turn inhibit the firing of the contralateral M [15–17]. This simple circuitry ensures that turns in response to threatening stimuli occur in a coherent, unidirectional manner.

We reasoned that mutants affecting electrical synapse formation could be identified relatively easily due to the simple and nearly stereotyped pattern of M/CoLo connections in the spinal cord. M and CoLo can be readily identified using the

transgenic line *Et(Tol-056:GFP)*, hereafter called *M/CoLo:GFP*, which expresses GFP in both types of neurons [18]. Most electrical synapses in the mammalian nervous system are composed of Cx36 [3]. The M circuit electrical synapses can be visualized by immunostaining with an antibody against the human Cx36 protein, which detects the zebrafish Cx36-related proteins [19]. The Cx36 staining apparent at the contact site of M and CoLo neurons is exclusively created by these two neurons, because laser ablation of either M or CoLo specifically eliminates the synapse (see Figures S1A–S1E and Table S1 available online).

We screened for mutations by creating gynogenetic diploid animals carrying random mutations generated by the chemical mutagen N-ethyl-N-nitrosourea (ENU) [20] and assessed the effect on electrical synapse formation by staining for Cx36 at 3 days postfertilization (dpf). We identified a mutation, which we called *disconnect4* (*dis4*), that caused a decrease in the amount of Cx36 at both sensory/M and M/CoLo synapses in the hindbrain and spinal cord, respectively (Figures 1B–1E; Table S2). In *nbea* mutants, there were normal numbers of M and CoLo neurons (average number of Ms per animal: WT = 2 ± 0, $dis4^{-/-}$ = 2 ± 0; CoLos per segment: WT = 1.97 ± 0.04, $dis4^{-/-}$ = 1.94 ± 0.05; n: WT = 18, *dis4* = 7), and their neurites contacted each other in the spinal cord as in wild-type (Figures 1E and 1E′). Mutants displayed no gross morphological defects in general body plan development or developmental timing and survived to at least 14 dpf but died before reaching adulthood. While neuronal ablation reduced Cx36 staining at M/CoLo synapses to background levels (Table S1), some Cx36 remained at *dis4* mutant synapses, but it was reduced by ~3 fold when compared to wild-type siblings (Figure 1F; Table S2). Mutants showed decreased levels of Cx36 staining in the M circuit from 3 to 14 dpf and also had decreased Cx36 staining at other prominent electrical synapses in the forebrain, midbrain, hindbrain, and spinal cord, suggesting a broad role for the mutated gene in electrical synaptogenesis (Figure 1 and data not shown).

To investigate whether there was diminished function at the electrical synapses in *dis4* mutants, we examined the passage of the gap junction-permeable dye Neurobiotin (Nb), which is known to move from the M axon into CoLo [18]. We retrogradely labeled M axons with Nb from a caudal spinal cord transection and then detected Nb within the CoLo cell bodies in the *M/CoLo:GFP* line. We found that in mutant animals, the amount of Nb transferred across gap junctions from M to CoLo was decreased ~3-fold as compared to the wild-type siblings (Figures 1G–1K; Table S2), similar to the decrease in the amount of Cx36 found at the synapse. Together, these data suggest that the gene mutated in *dis4* animals is required for electrical synapse formation and function.

neurobeachin Is Required for Electrical Synapse Formation

We mapped the *dis4* mutation using our recently developed RNA sequencing (RNA-seq)-based mapping method [21]. The method is based on a bulk segregant analysis approach in which shared regions of genomic homozygosity can be identified in a pool of mutant animals. We pooled 80 mutant (−/−) and 80 wild-type (+/+ and −/+) siblings and extracted and sequenced mRNA (Illumina Hi-Seq) from each pool. The sequence was aligned to the genome, and SNPs were identified in the wild-type pool that would serve as mapping markers. The SNP allele frequencies were then examined at the marker positions in the mutant pool, identifying a linked region of ~2.5 Mb on chromosome 10 (Figures 2A and 2B). Within this region, we used the RNA-seq data to identify candidate mutations and found one nonsense mutation that truncates the gene *neurobeachin* (*nbea*) at aa 906, eleven missense changes in other genes, and two genes in the interval, including *nbea*, that had a significantly reduced expression in mutant as compared to wild-type; the decrease in *nbea* is consistent with nonsense-mediated decay (Figures 2C and 2D). To test whether the nonsense mutation in *nbea* was responsible for the mutant phenotype, we generated two frame-shifting deletions in *nbea* using transcription activator-like effector nucleases (TALENs) [22]: a 7 bp deletion in the first exon ($nbea^{fh392}$) and an 8 bp deletion in exon 21 ($nbea^{fh380}$) overlapping the location of the ENU-induced *dis4* mutation (Figure 2E). Both $nbea^{fh392}$ and $nbea^{fh380}$ failed to complement the *dis4* mutation, and all mutant allelic combinations resulted in the same ~3-fold reduction in Cx36 staining at M/CoLo synapses (Figure 2F), suggesting that all alleles are null. For all further analysis, we used the *dis4* allele, which we renamed $nbea^{fh364}$.

Nbea is a large multidomain scaffolding protein and is highly conserved within vertebrates (Figures 2E and 2G) [10]. It is expressed throughout the nervous system in human [23], mouse [9, 10], and zebrafish [24] and localizes to tubulovesicular membranes found near the Golgi, in dendrites and axons, and close to the synapse [10]. We found Nbea protein staining throughout the zebrafish nervous system with a punctate distribution within neuronal cell bodies and extending into the neurites, similar to that described in mouse [10, 11]; this staining was lost in mutants, further supporting the idea that the $nbea^{fh364}$ mutation is a null allele (Figure S2). In zebrafish there are two *nbea* genes, *nbeaa* and *nbeab*; the mutations we have identified and created are in *nbeaa* (referred to throughout as *nbea*), which is most closely related to the human and mouse *nbea* genes (Figure 2G, percent of identical amino acids compared to human: nbea = 84, nbeab = 81). *nbeab* is unlikely to have a major role, as RNA-seq analysis showed that *nbeab* is expressed at an ~10-fold lower level than *nbea* in wild-type animals (*nbea* = 7.87, *nbeab* = 0.76, fragments per kilobase of transcript per million mapped reads). We conclude that Nbea is required for electrical synaptogenesis.

Nbea Is Required for Glycinergic Synapse Formation

nbea mutant mice have morphologically and functionally defective glutamatergic and GABAergic chemical synapses [11–13], analogous to the defects we see at electrical synapses. While Nbea has been found to biochemically interact with glycine receptors [25], it has not been shown to be required for glycinergic synapse formation. We therefore examined the glycinergic synapses that form onto the M circuit to determine whether Nbea was required for their formation. M receives extensive glycinergic input on its dendrite and cell body and expresses glycine receptor (GlyR), which can be detected using immunostaining (Figure 3) [26]. In the spinal cord, we found GlyR staining that localized adjacent to the M/CoLo electrical synapse, and this staining was localized either with the main crossing CoLo axon or with thin processes that branched from CoLo's main axon. These latter processes are often not visible in images due to their fasciculation with the very large and bright M axon (a visible example is shown in Figure S1G, double arrowhead). The GlyR staining that is near the M/CoLo electrical synapse likely represents CoLo/CoLo inhibitory synapses [15, 18]. Ablating M led to a loss of GlyR staining associated with M dendrites in the hindbrain but had no effect

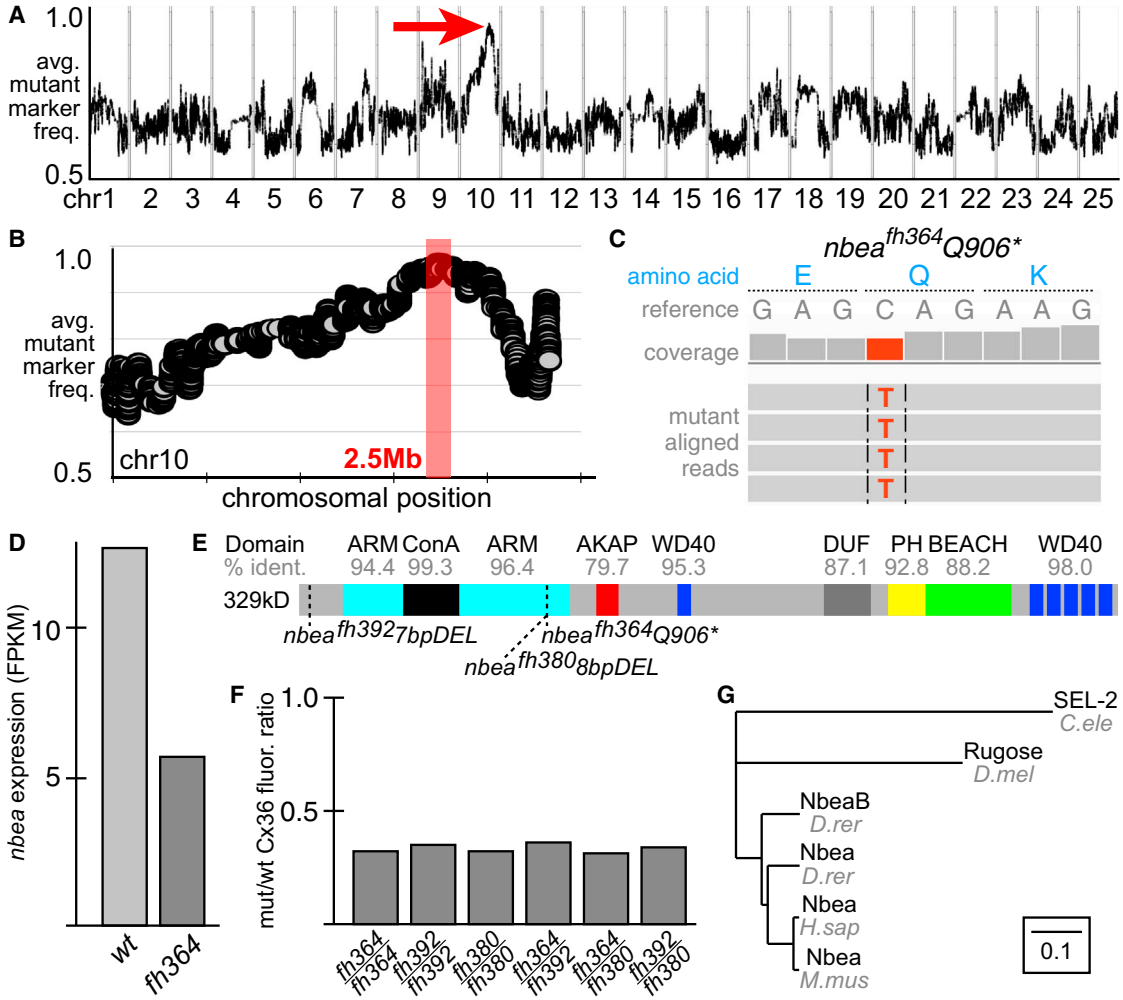

Figure 2. The *dis4* Mutation Disrupts *neurobeachin*

(A) Genome-wide RNA-seq-based mapping data. The average frequency of mutant markers (black marks) is plotted against genomic position. A single region on chromosome 10 (chr10) emerges with an allele frequency near 1.0, indicating linkage to the *dis4* mutation (red arrow). Each chromosome is separated by vertical lines and labeled at the bottom.

(B) Detail of chr10. The average frequency of mutant markers (gray discs) is plotted against chromosomal position. The red bar marks the region of tightest linkage. Each tick mark on the x axis represents 10 Mb.

(C) Mutant reads are shown aligned to the reference genome, identifying a C-to-T transition in *neurobeachin* (*nbea*) creating a nonsense mutation at amino acid 906. Aligned reads are shown as gray boxes; differences from reference are highlighted by colored letters.

(D) *nbea* is downregulated presumably due to nonsense-mediated decay (Cufflinks, $\log_2$ fold change = −0.82).

(E) Illustration of the primary structure of Nbea, with protein domains depicted as colored boxes. The homology of zebrafish to human domains is labeled (% ident.), and the locations of the mutations are marked by dashed lines.

(F) Ratio of mutant to wild-type Cx36 fluorescence at M/CoLo synapses for each allelic combination listed. Wild-type animals were siblings (homozygous and heterozygous) from a given cross. Data for *fh364/fh364* are derived from that in Figure 1F.

(G) Phylogenetic tree depicting relationships among Nbea gene family in common multicellular model organisms. Scale bar represents substitutions per site.

on the staining associated with the presumed CoLo/CoLo sites of contact in the spinal cord (Figures S1F, S1G, and S1J). If the two CoLos in the same segment are indeed forming synapses with one another, then each CoLo is both postsynaptic on its ipsilateral side of the spinal cord and presynaptic on its contralateral side (see diagram in Figure 1A). We found that ablating CoLo caused the GlyR punctae on the ablation side (i.e., postsynaptic; arrow, Figure S1I) to be reduced to background levels (Figure S1J; Table S1). On the side opposite the ablation (i.e., presynaptic; arrowhead, Figure S1I), there is an ~35% decrease in the intensity of the GlyR staining (Figure S1J; Table S1). We conclude that GlyR punctae found adjacent to the M/CoLo electrical synapse are associated with CoLo/CoLo inhibitory synapses.

Having established that the GlyR staining observed can be attributed to particular neurons of the M circuit, we examined the effects of removing Nbea on glycinergic synapse formation. In mutants, GlyR staining was diminished at both Mauthner hindbrain and CoLo/CoLo synapses (Figures 3A–3D). At *nbea* mutant CoLo/CoLo synapses, the amount of GlyR localized at the synapse was decreased ~2-fold when compared to wild-type siblings (Figure 3E). Mutants showed reduced GlyR staining from 3 to 14 dpf, and GlyR staining, which is found predominantly in the hindbrain and spinal cord, was

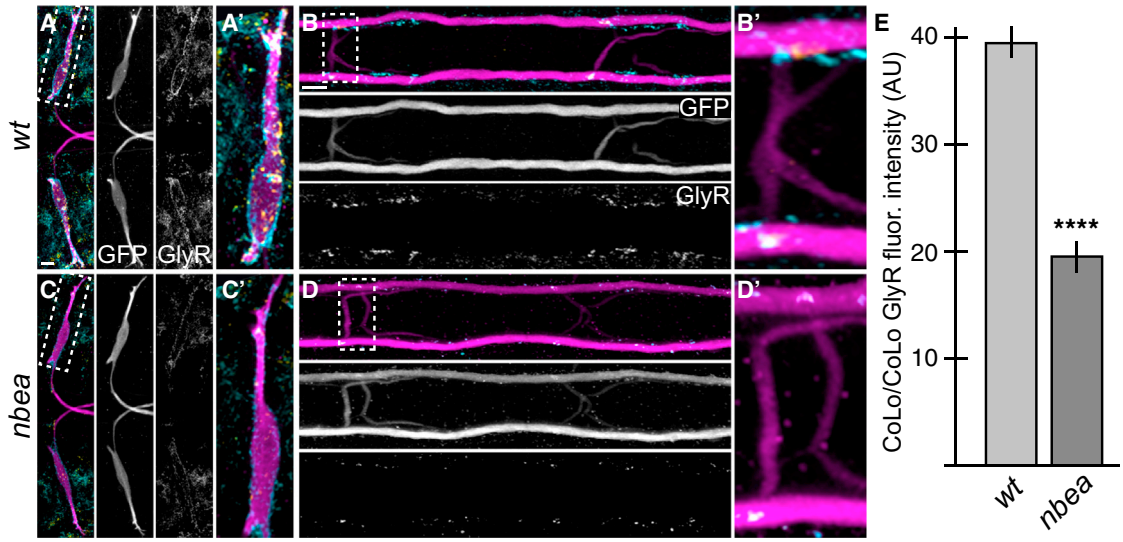

Figure 3. Glycinergic Synapses Are Disrupted in *nbea* Mutants

Larvae were stained for GFP (magenta), Cx36 (yellow), and glycine receptor (GlyR, cyan). Individual GFP and GlyR channels are shown in neighboring panels. (A–D) The GlyR staining found on M dendrites (A) and CoLo/CoLo synapses (B) is diminished in *nbea* mutant animals (C and D).

(E) Quantitation of the amount of GlyR in wild-type and mutant CoLo/CoLo synapses. See Figure 1A for circuit diagram. Graphs represent data as mean ± SEM. ****$p < 0.0001$ compared to control.

Associated experimental statistics are found in Table S2.

reduced across all regions in *nbea* mutants (Figure 3 and data not shown). The M neuron also receives glutamatergic and GABAergic input; we attempted to visualize these synaptic types by staining for their receptors but could not find suitable antibodies to recognize them. By contrast, when we visualized presynaptic markers (Synapsin, SV2) at central synapses or neuromuscular junctions, we found no defects in *nbea* mutants (Figure S3). Mice that are heterozygous for a *nbea* mutation have defects in the size and function of synapses [13]. We found no defects in heterozygous fish (+/*fh364*) at glycinergic or electrical synapses (Table S2). We conclude that *nbea* is required for glycinergic synapse formation.

Nbea Is Required for Synaptic Scaffold Localization

Previous reports suggested that synaptic scaffolds were unaffected in *nbea* mutant mice [11]; however, Nbea has been suggested to interact with the glutamatergic scaffold SAP102 directly [27]. We first examined the localization of the electrical synapse scaffold ZO-1, which is known to interact through its PDZ domain with the C terminus of Cx36 [28]. We found that ZO-1 was colocalized with Cx36 within the M circuit as well as at other prominent electrical synapses (Figures 4A and 4B). Additional ZO-1 staining was found at nonsynaptic tight junctions (Figure 4 and data not shown). In *nbea* mutants, ZO-1 was reduced at all electrical synapses (Figures 4C and 4D), but this reduction was less pronounced than the reduction of Cx36 (compare Figure 4E and Figure 1F; see also Table S2). We next examined the glycinergic scaffold Gephyrin (Geph), which is the main scaffold found at GABAergic and glycinergic inhibitory synapses [29]. In wild-type, there was extensive colocalization of GlyR and Geph within the M circuit as well as more broadly across the hindbrain and spinal cord (Figures 4F and 4G and data not shown). In *nbea* mutants, Geph was reduced at all synapses (Figures 4H and 4I); however, similar to the electrical synapse, the reduction of the scaffold was less pronounced than the reduction of GlyR (compare Figure 4J and Figure 3E; see also Table S2). We conclude that the transmembrane proteins Cx36 and GlyR of the synapse are more dependent on Nbea function than the cytosolic scaffolds are.

nbea Mutant Animals Have Reduced Behavioral Performance

We next asked whether the synaptic defects observed in *nbea* mutants resulted in impaired functionality of the nervous system. The M circuit is one of the first neural circuits to wire and respond in young zebrafish and drives a fast escape response to startling vibrational stimuli at 6 dpf [16]. The M neuron has "segmental homologs" in more posterior hindbrain segments that also contribute to the escape response [30]. M is required for short latency escapes (~10 ms), while the homologs drive similar but longer latency responses (~18 ms) [31, 32]. We created a behavioral testing apparatus consisting of an open arena in which free-swimming animals were confronted with vibrations created from a nearby speaker [18]. Using high-speed videography, we found that wild-type animals at 6 dpf responded to a 500 Hz, 10 ms tone with escape responses (Figure 5A). Animals showed no directional bias escaping either to the left or right with both short- and long-latency escapes [18]. We found that *nbea* mutant animals responded with escapes less than half as frequently as their wild-type (+/+ and +/−) siblings or as compared to a wild-type stock from our facility (Figures 5B–5E; Table S3). Each animal was tested for its response to the tone in three separate trials. Although *nbea* mutants responded in fewer trials than their wild-type counterparts did, mutants could perform escape responses that were indistinguishable from wild-type (Figures 5A and 5D). The behavioral defects observed were not confined to the escape response, as *nbea* mutant animals were frequently found lying on their sides (Figures 5C and 5F). The balance defect was not due to a lack of swim bladders, which in mutants formed at 5 dpf, similar to their wild-type

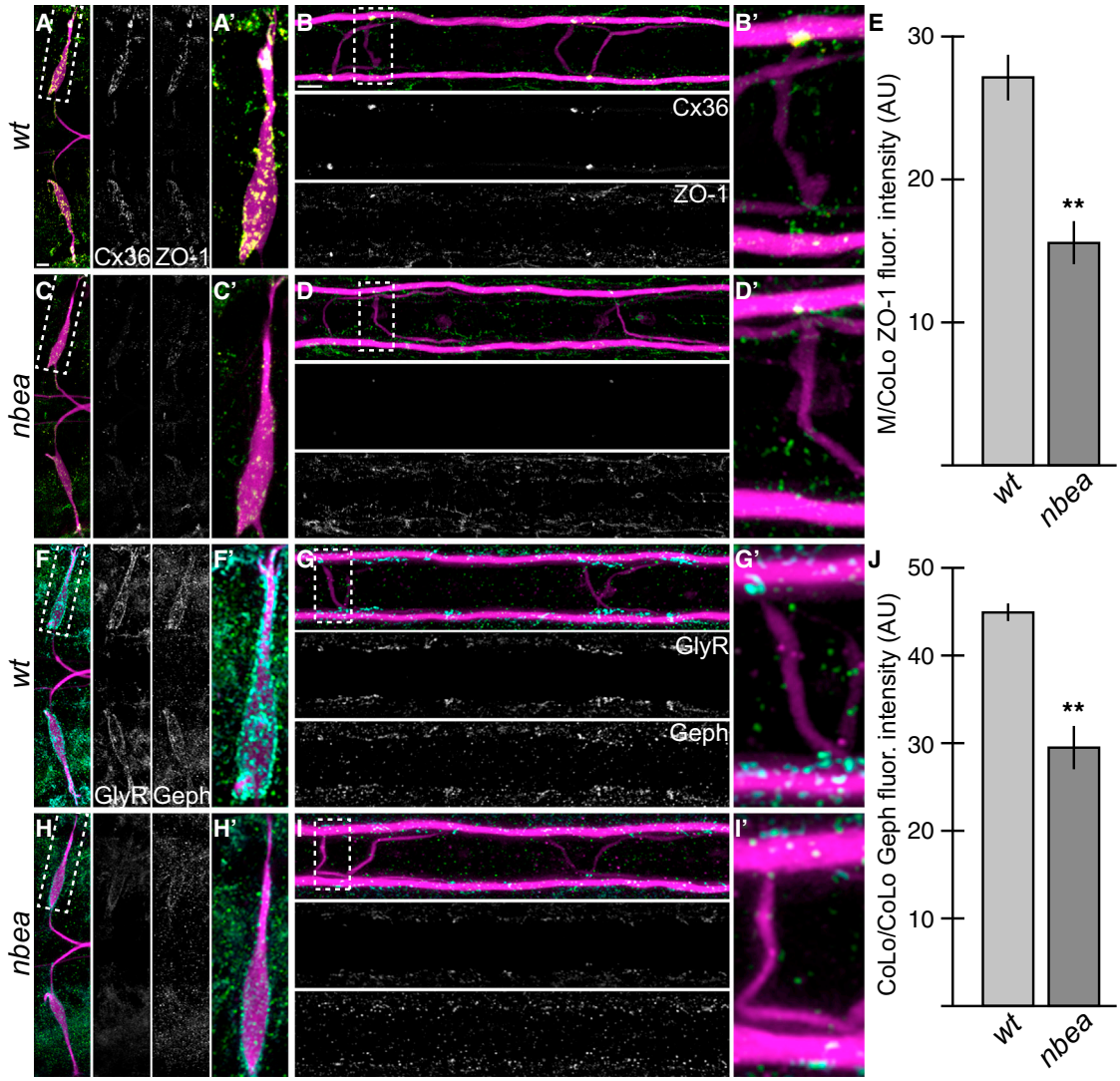

Figure 4. Electrical and Chemical Synaptic Scaffolds Are Disrupted in *nbea* Mutants

(A–D and F–I) Larvae are stained for GFP (magenta) in all panels, Cx36 (yellow) and ZO-1 (green) in (A)–(D), and GlyR (cyan) and Gephyrin (Geph, green) in (F)–(I). Individual Cx36, ZO-1, GlyR, and Geph channels are shown in neighboring panels. Note that for each spinal cord zoom, there is only one M/CoLo and CoLo/CoLo synapse depicted; this is due to natural variation in the positions of CoLo neurons in the spinal cord.

(A–D) The electrical synapse scaffold ZO-1 is colocalized with Cx36 at M dendritic (A and A′) and spinal cord (B and B′) synapses. ZO-1 staining is diminished in mutants (C and D), but less severely than Cx36.

(E) Quantitation of ZO-1 at M/CoLo synapses in wild-type and *nbea* mutants.

(F–I) The inhibitory synapse scaffold Geph is colocalized with GlyR at M dendritic (F and F′) and CoLo spinal cord (G and G′) synapses. Geph staining is diminished in mutants (H and I), but less severely than GlyR.

(J) Quantitation of Geph at CoLo/CoLo synapses in wild-type and *nbea* mutants.

Graphs in (E) and (J) represent data as mean ± SEM. **p < 0.01 compared to control.

Associated experimental statistics are found in Table S2.

siblings, and did not explain the decreased escape response, as animals on their side could respond to the tone. By 6 dpf, wild-type animals actively corrected their balance using their pectoral fins, whereas *nbea* mutants often failed to correct their balance when they began to fall. Additionally, we found that mutants were less sensitive to touch, displayed decreased overall motion, and were generally less reactive than their wild-type counterparts (Movies S1 and S2). However, in all types of behavior, when mutant animals responded they did so with what appeared to be normal coordination, analogous to what we observed in the escape response. We conclude that the loss of *nbea* leads to broad behavioral deficits that do not prevent normal behavior but decrease its normal occurrence.

Nbea Is Required Autonomously by the Postsynaptic Neuron for Electrical and Chemical Synapse Formation

Because Nbea is expressed throughout the nervous system, it is unclear whether it functions in the pre- or postsynaptic neuron, or both. Indeed, in mice mutant for *nbea*, there are defects on both sides of the synapse, with fewer synaptic vesicles presynaptically and a reduced size of the postsynaptic density [11–13]. To test whether Nbea functions in the pre- or postsynaptic neuron in vivo, we wanted to create mosaic

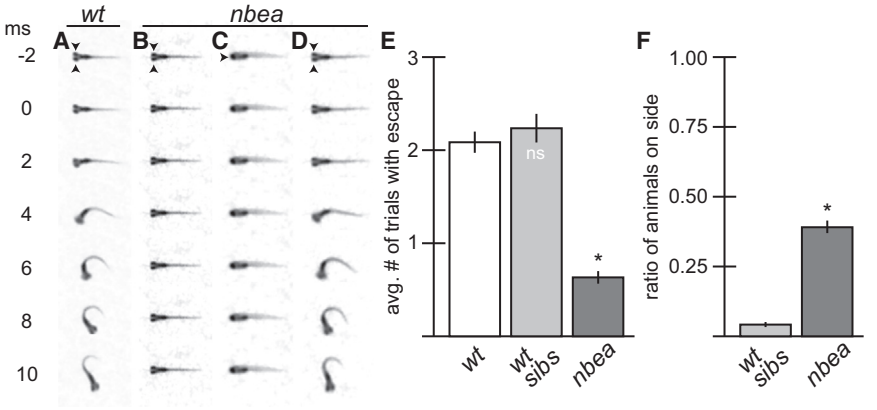

Figure 5. *nbea* Mutants Have Defects in Eliciting Normal Behavior

(A–D) Individual frames from a 500 fps movie. Arrowheads point to eyes. Auditory startle stimulus was applied at time = 0 (ms = millisecond).

(A) M is responsible for a fast-escape response to threatening stimuli and initiates a turn away from stimulus that is completed in 10 ms.

(B–D) *nbea* mutant animals often fail to initiate turns (B) and are frequently found lying on their side (C). However, when they do respond, the behavior produced is indistinguishable from wild-type (D).

(E and F) Quantitation of escape response and balance defects in a separate wild-type line (wt), *nbea* mutant animals, and their wt siblings (wt sibs). Each animal was tested in three separate trials for its response to stimulus. The average number of trials with response (E) or with animals on their sides (F) was recorded. Graphs represent data as mean ± SEM from three separate trials.

*p < 0.05 compared to control; ns, not significant.

Associated experimental statistics are found in Table S3.

animals containing wild-type and mutant cells and examine which required Nbea. We therefore transplanted cells from an *M/CoLo:GFP* donor into an unmarked host embryo at the blastula stage and examined the resulting embryos at 6 dpf (Figure 6) [33]. In the transplant experiments, chimeric animals were identified with only GFP-marked M, only GFP-marked CoLos, or both; in the case of M, we only found examples where a single M was marked with GFP, while the number of GFP-marked CoLos in a chimera ranged from 1 to 13 (average = 3, n = 75; there are ~60 total CoLos per animal). In control transplants, there was no effect on Cx36 localization at M/CoLo synapses when comparing synapses associated with GFP-marked and unmarked neurons (Figures 6A–6C and 6J). To test where *nbea* was required, we transplanted cells from *nbea* mutant, *M/CoLo:GFP* donors into wild-type hosts. When the postsynaptic CoLo was *nbea* mutant, the Cx36 staining at the M/CoLo synapse decreased by ~2.5-fold, whereas when the presynaptic M axon was mutant, there was only an ~20% decrease (Figures 6E, 6F, and 6J). When both the pre- and postsynaptic neurons were *nbea* mutant, the decrease in Cx36 was ~3-fold (Figure 6J; Table S4), similar to the homozygous mutant phenotype (Figure 1). Analogous to the postsynaptic requirement of Nbea in CoLo, we found that when M is *nbea* mutant in a wild-type host, it loses its synapses in the hindbrain; these synapses are postsynaptic to the incoming sensory input (Figure 6D). We conclude that Nbea is required mainly postsynaptically for electrical synapse formation.

We next asked whether Nbea was sufficient for electrical synapse formation and so created chimeras in which cells from wild-type, *M/CoLo:GFP* embryos were transplanted into unmarked *nbea* mutant hosts. We found that when the postsynaptic CoLo was wild-type in a mutant host, the M/CoLo synapse was rescued with a >3-fold increase in Cx36 fluorescence compared to the mutant synapses within the same animals (Figures 6I and 6K). By contrast, when the presynaptic M axon was wild-type in a mutant background, there was no rescue of Cx36 (Figures 6H and 6K). Similar to the postsynaptic sufficiency of Nbea in CoLo, when M is wild-type in an otherwise *nbea* mutant animal, the Cx36 associated with electrical synapses on its postsynaptic dendrites and cell body in the hindbrain is rescued (Figure 6G). Moreover, Nbea's postsynaptic rescue of Cx36 at the synapse is not enhanced when the presynaptic neuron is also wild-type (Figure 6K). We conclude that Nbea is sufficient postsynaptically for electrical synaptogenesis.

We next asked whether Nbea was required postsynaptically for glycinergic chemical synapse formation and so examined the chimeras for GlyR localization. At the CoLo/CoLo synapses, removing *nbea* from the postsynaptic neuron caused a decrease in GlyR fluorescence by ~2 fold, whereas removal from the presynaptic neuron had no effect (Figures 6C, 6F, and 6L; Table S4); moreover, there was no additive effect when both the pre- and postsynaptic neurons were mutant (Figure 6L; Table S4). The decrease in GlyR fluorescence when removing *nbea* from the postsynaptic CoLo was similar to that of the homozygous mutants (Figure 3). Likewise, when M was *nbea* mutant in a wild-type animal, the GlyR staining on its postsynaptic dendrites in the hindbrain was reduced (Figure 6D). We found that Nbea was also sufficient in the postsynaptic neuron (be it CoLo or M), but not in the presynaptic neuron, to rescue GlyR localization (Figures 6G–6I and 6M; Table S4). Taking these results together, we conclude that Nbea is both necessary and sufficient within the postsynaptic neuron for electrical and chemical synapse formation.

Nbea Is Required Autonomously for Dendritic Complexity

While the major patterns of neural architecture were unaffected in *nbea* mutants (Figures 1, 3, and 4), we found that there were defects specifically in the fine terminal branches of M's dendritic arbor. The M neuron elaborates two main dendritic branches, the lateral dendrite that receives input from sensory neurons and the extensively branched ventral dendrite that receives descending input from higher levels of the brain; M also extends additional fine dendritic processes from the M soma [34]. We found that at 5 dpf, *nbea* mutants have normal axonal development (Figures 1, 3, and 4) but reduced dendritic complexity (Figure S4). Analyzing the chimeras, we found that *nbea* is required autonomously by the postsynaptic neuron for dendritic elaboration (Figures 7A and 7B). When M is *nbea* mutant in a wild-type host, the length of its main dendritic branch is unaffected (Figure 7D) but the total arbor length is decreased, correlating with fewer branches (Figures 7E and 7F; Table S5). In particular, the fine terminal dendritic branches are lost, with the primary, secondary, and tertiary remaining (Figure 7G). Furthermore, Nbea was sufficient autonomously in the postsynaptic neuron for the elaboration of fine dendritic arbors since a wild-type M in an

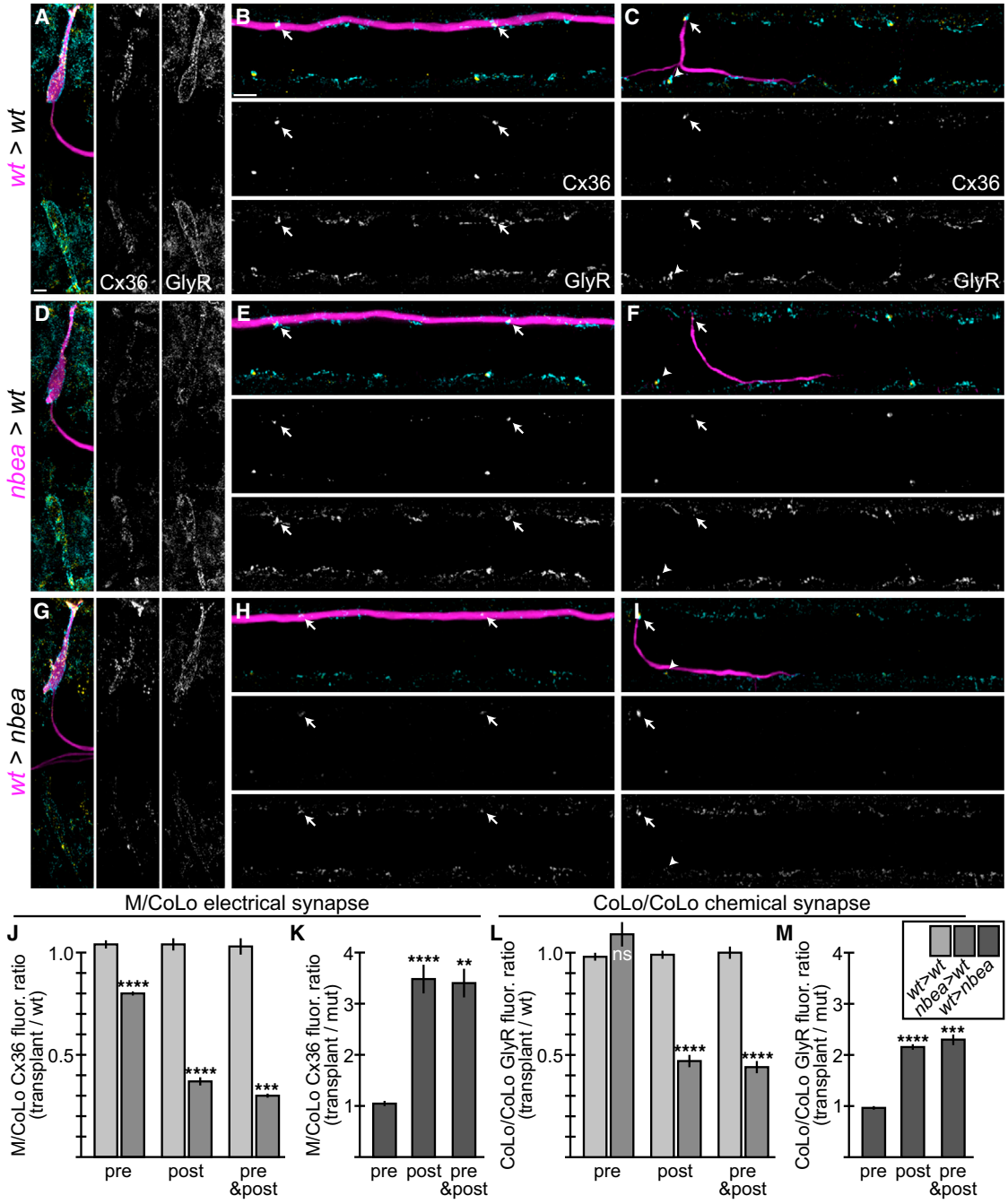

Figure 6. Neurobeachin Is Necessary and Sufficient in the Postsynaptic Neuron for Electrical and Chemical Synapse Formation

(A–I) Dorsal views of chimeric larvae at 6 dpf containing GFP-marked cells transplanted from an *M/CoLo:GFP* embryo into an unmarked host. Larvae are stained for GFP (magenta), Cx36 (yellow), and glycine receptor (GlyR, cyan). Individual Cx36 and GlyR channels are shown in neighboring panels. Arrows point to M/CoLo electrical synapses. Arrows also point to the adjacent postsynaptic side of the CoLo/CoLo synapse associated with the upper left CoLo neuron. Arrowheads point to the presynaptic side of the glycinergic synapse associated with the upper left CoLo neuron.

(A–C) Individual examples of control chimeric larvae with cells transplanted from a *M/CoLo:GFP* embryo into an unmarked wild-type host (*wt>wt*).

(D–F) Examples of chimeric larvae testing where Nbea is necessary, with cells transplanted from a *nbea* mutant *M/CoLo:GFP* embryo into an unmarked wild-type host (*nbea>wt*). Note the greatly diminished synapses when the *nbea* mutant cell is the postsynaptic neuron (D and F).

(G–I) Examples of chimeric larvae testing where Nbea is sufficient, with cells transplanted from an *M/CoLo:GFP* embryo into an unmarked *nbea* mutant host (*wt>nbea*). Note that synapses are rescued when the postsynaptic neuron is wild-type for Nbea (G and I).

(J–M) Quantitation of the ratio of Cx36 fluorescence at M/CoLo or GlyR fluorescence at CoLo/CoLo synapses at transplant-associated neurons compared to unassociated neurons within the same animal in *wt>wt* and *nbea>wt* chimeras (J and L) and *wt>nbea* chimeras (K and M). Graphs represent data as mean ± SEM. **p < 0.01, ***p < 0.001, ****p < 0.0001 compared to control; ns, not significant.

Associated experimental statistics are found in Table S4.

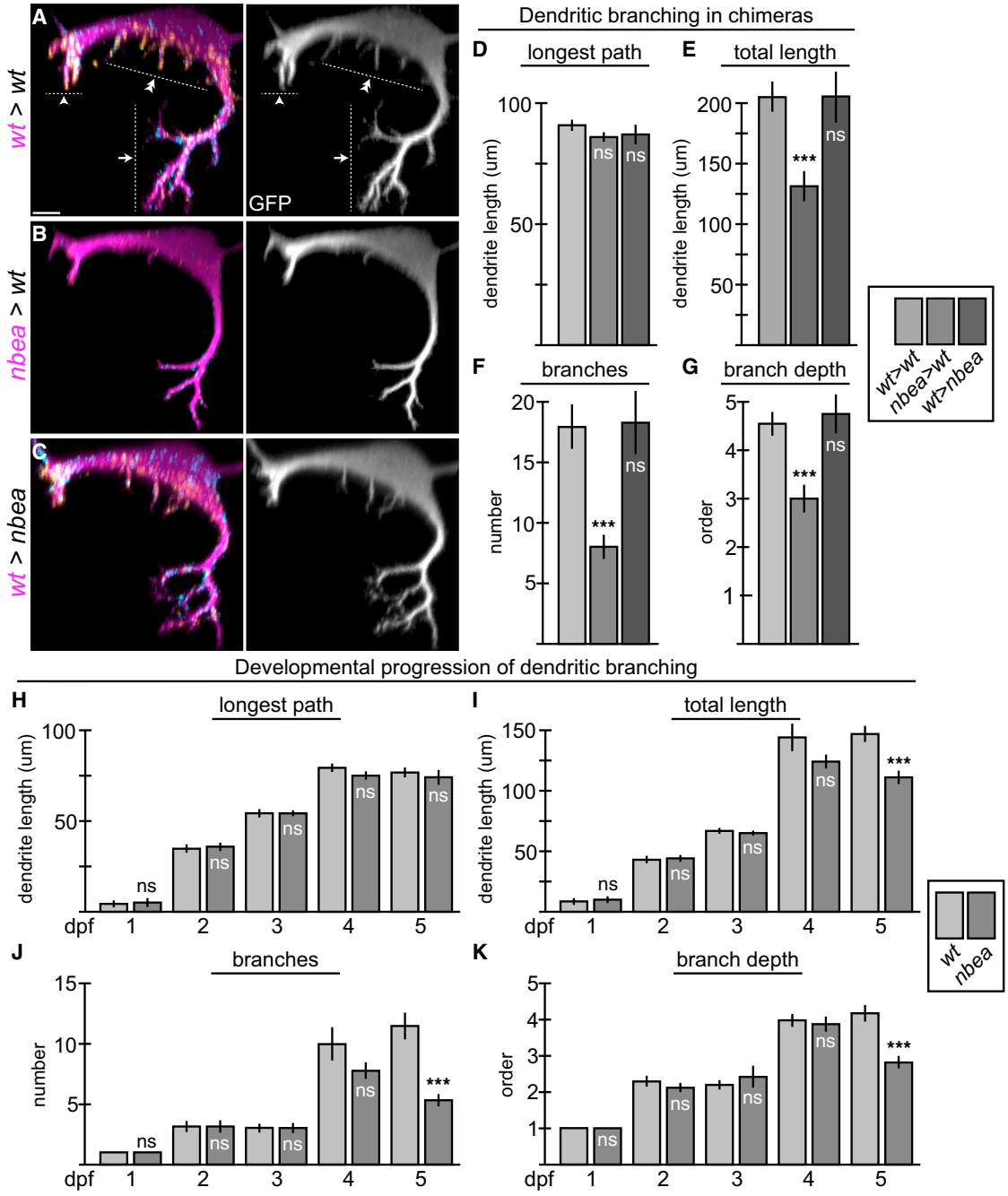

Figure 7. Neurobeachin Is Required Autonomously to Maintain Dendritic Complexity

(A–C) Cross-section views of individual chimeric larvae containing GFP-marked cells from *M/CoLo:GFP* embryos in unmarked hosts at 6 dpf. Images are maximum-intensity projections of ~20 μm from digitally rendered cross-sections. For clarity, fluorescence signal outside of the GFP-labeled neurons has been digitally removed. Ventral is down, lateral is to the left. Scale bar represents 10 μm. Larvae are stained for GFP (magenta), Cx36 (yellow), and GlyR (cyan). The GFP channel is shown in neighboring panels.

(A) In wild-type (*wt>wt*), M elaborates complex dendrites with three main compartments: ventral (arrow), lateral (arrowhead), and somatic (double arrowhead).

(B) When M is *nbea* mutant in an otherwise wild-type host (*nbea>wt*), the M dendrites lose the fine terminal branches of the dendritic arbor.

(C) When M is wild-type in a *nbea* mutant host (*wt>nbea*), the dendritic complexity is similar to wild-type.

(D–G) Quantitation of M ventral dendrite parameters in chimeric embryos.

(H–K) Quantitation of changes in the ventral dendrite from 1 to 5 dpf in wild-type and *nbea* mutant embryos. "Longest path" is the longest continuous main path from cell body to dendrite tip. "Total length" is the sum of the lengths of all the dendritic branches. "Branches" is the sum of the number of branches made off of the main, longest branch. "Branch depth" is the maximum depth of branching, with the main branch being primary and all subsequent branches being labeled sequentially.

Graphs in (D)–(K) represent data as mean ± SEM. ***$p < 0.001$ compared to control; ns, not significant.

Associated experimental statistics are found in Table S5.

otherwise *nbea* mutant host acquires the dendritic complexity of control transplants (Figures 7C–7G; Table S5). The ventral dendrite data are summarized in Figures 7D–7G, but similar trends were found in the lateral and somatic dendrites as well (Table S5). We conclude that Nbea is required autonomously for dendritic arborization.

We wondered whether the dendritic arborization phenotype was due to defects in the initiation of dendritogenesis or instead in the maintenance of the dendritic arbor. Because the M dendrites are not accessible to live imaging, we examined M dendrite formation using fixed stages from 1 to 5 dpf in *nbea* mutants and wild-type siblings. In wild-type, all M dendrites begin outgrowth at approximately 1 dpf, with the primary branches growing substantially in the next 3 days and becoming stable between 4 and 5 dpf. However, at this time there is a large increase in the total dendritic arbor size correlated with an increase in the number of branches. In *nbea* mutants, the initial outgrowth and branching of dendrites is unaffected and they are able to generate a complex, branched arbor with fine dendritic branches initially (1–4 dpf; Figures 7H–7K and S4; Table S5). However, they cannot maintain the fine processes, resulting in a loss of complexity (5 dpf; Figures 7H–7K and S4). Taken together, these results suggest that Nbea is not required for initiating dendritic complexity but is instead required to maintain the extensive branching and fine dendritic processes found in mature neurons.

Discussion

Here, using the power of forward genetics in zebrafish coupled with the identified synapses of the M neural circuit in vivo, we find that Nbea is required for electrical synapse formation and function. Little is known about the genes required for electrical synaptogenesis, but the structural differences between electrical and chemical synapses suggest that unique mechanisms would be used for their construction. Thus, Nbea's involvement in electrical synaptogenesis was surprising given its known role in glutamatergic and GABAergic chemical synapse formation in mice [9, 11–13]. We also find that Nbea is required for chemical synapse formation in zebrafish and broaden Nbea's role still further by showing that it is required for glycinergic chemical synaptogenesis. Our work, together with work in mice, suggests that Nbea is required for the formation of the major forms of synaptic communication within the nervous system. We also find that Nbea is dispensable for axon formation but is required to maintain the terminal branches of M's dendritic arbor. Critically, using chimeric analysis in vivo, we find that Nbea is necessary and sufficient in the postsynaptic neuron for electrical and chemical synaptogenesis and dendritic arborization. Our analysis relies mainly on immunofluorescence staining and quantitation of electrical and chemical synaptic components, which have limitations in terms of estimating the phenotypic severity observed. However, we note that our analysis is consistent across experiment types (e.g., homozygous mutants and chimeras). Moreover, we show corresponding functional defects at the electrical synapses using Neurobiotin passage as our measure. And ultimately, the synaptic defects we observed in mutants correlate with deficits in the ability to initiate behavior with normal frequency. Taken together, our findings identify Nbea as a broad postsynaptic regulator of synapse formation, with its loss leading to a severely underconnected and underperforming nervous system.

Whether Nbea functions in the pre- or postsynaptic neuron to facilitate synaptogenesis has until now been controversial. Presynaptic function for Nbea is supported by the findings that in *nbea* mutant mice, there is a loss of evoked neurotransmitter release at neuromuscular junctions and central synapses correlated with decreased numbers of SVs and levels of presynaptic proteins [9, 12]. By contrast, postsynaptic Nbea function was ascribed to decreased size of the postsynaptic density in *nbea* mutant mice and defects in dendritic spine formation in *nbea* mutant cultured neurons [11, 13]. Given that Nbea is expressed throughout the nervous system, and since feedback between the pre- and postsynaptic neurons is critical for robust synaptogenesis [35], these results have not delineated the primary site of Nbea function. Our results using chimeric analysis in vivo demonstrate unambiguously that Nbea is required in the postsynaptic neuron for both electrical and chemical synapse formation. Consistent with our findings, in two-neuron coculture assays Nbea was required in the postsynaptic neuron for synaptic function [11]. We did find a minor presynaptic requirement for Nbea in electrical, but not chemical, synapse formation, leaving open the possibility of presynaptic Nbea function. However, we find that Nbea is sufficient for synaptogenesis only when present postsynaptically in an otherwise mutant animal. That is, even when the presynaptic neuron is mutant, Nbea in the postsynaptic neuron is able to rescue synaptogenesis. Our results suggest that Nbea's main cell biological role is performed in the dendrites of neurons, where it broadly controls electrical and chemical synaptogenesis.

Chemical synapses are inherently asymmetric structures. Synaptic vesicles are poised for release near the active zone presynaptically, while neurotransmitter receptors and associated scaffolds reside postsynaptically [2, 35]. Therefore, it is unsurprising to identify a molecule such as Nbea that is required exclusively postsynaptically for chemical synapse formation. In contrast to chemical synapses, electrical synapses are often viewed as overtly symmetrical structures, being composed of identical hexamers of Cxs contributed by the pre- and postsynaptic neurons [3]. Yet, recent results show that electrical synapses can be molecularly asymmetric, with unique pre- and postsynaptic Cxs [19]. Indeed, we have found that different Cx36-related proteins are required pre- and postsynaptically in the zebrafish M circuit for electrical synapse formation (A.C.M. and C.B.M., unpublished data). That Nbea, a putative vesicle-trafficking protein, acts postsynaptically suggests that it may function in the dendritic targeting of postsynaptic Cx proteins at molecularly asymmetric electrical synapses. Moreover, Nbea biochemically interacts with synaptic scaffolds [27], and we show that it is required for scaffold accumulation at synapses, suggesting that electrical synapse asymmetry may extend beyond the Cxs, analogous to chemical synapse structure. While Cx regulation can affect electrical synapse function [5], asymmetry of the entire macromolecular complex including the synaptic scaffolds would represent an important new form of control for gap junctional coupling between neurons.

It is widely observed that synapse formation occurs simultaneously with neuronal arborization [1]. Here we find that Nbea is necessary and sufficient in the postsynaptic neuron for both synapse formation and maintaining dendritic complexity. Our findings support a role for Nbea as an important coordinator of synaptogenesis with dendritic arborization, but how this coordination is achieved is unclear. It could be that the loss of neurotransmitter receptors observed in *nbea* mutants causes the correlated loss of dendritic complexity. For example, in *Xenopus* tectal neurons, blocking NMDA receptor recruitment

to nascent synaptic sites causes defects in dendritic arborization [36]. Alternatively, the absence of electrical synapses, themselves inherently adhesive structures [37], might contribute to the destabilization of terminal dendritic branches and their subsequent loss. In line with these possibilities, we found that electrical and chemical synapses were diminished in mutants before we detected changes in dendritic morphology. In contrast to our results, physically ablating sensory input to M early during development resulted in severely reduced dendrites lacking secondary, tertiary, and terminal branches as well as causing a failure of primary outgrowth in some cases [38]. This suggests that M dendritic arborization occurs in multiple stages with a number of interacting mechanisms and that Nbea's function occurs after initial contact-mediated support provided by afferent neurons. Together, our results identify Nbea as an important coordinator of synapse formation and dendritic complexity, yet how it controls these related processes remains unknown.

The favored model for Nbea's function is that it controls the trafficking of synaptic proteins directly. The family of BEACH-domain-containing proteins, to which Nbea belongs, play roles in vesicle trafficking, membrane dynamics, and receptor signaling [6]. Nbea's localization to vesicular structures found near the *trans*-face of the Golgi and dendrites suggests a role in trafficking [10]. In support of this idea, recent work showed that when *nbea* was removed from cultured neurons, the surface expression, but not the overall level, of glutamate and GABA receptors was reduced, with correlated increases in the level of receptors trapped in the ER and/or Golgi [11]. In keeping with these results, we found that there were defects in the localization of the transmembrane receptors (Cxs and GlyR) and the cytosolic scaffolds (ZO-1 and Geph) at electrical and chemical synapses, respectively. If the Nbea vesicle-trafficking model is correct, then either Nbea must control very disparate vesicle types (both electrical and chemical receptor-containing vesicles), or else a common dendritically targeted vesicle may be involved. However, the nature of the vesicles on which Nbea localizes is uncertain. Costaining of Nbea and endomembrane markers has found that it localizes adjacent to the ER-Golgi complex in the cell body, with the best overlap with the SNARE protein Vti1A, whereas in dendrites it is most associated with recycling endosomes [11]. Yet, Nbea punctae are associated with the recycling endosome in only half of cases, suggesting a transient interaction with this compartment. Future experiments will be required to identify the mechanistic basis by which Nbea regulates synaptogenesis.

Although Nbea's molecular function is currently unclear, deletions and point mutations in Nbea have been linked to patients with autism spectrum disorder (ASD) [6–8]. Autism is a complex neurodevelopmental disorder controlled by hundreds of genes, yet the pathways identified converge on synapse formation and neural circuit function [39]. Our findings suggest that defects in electrical synapse formation and function could be an underlying factor contributing to ASD. While we have focused on electrical synapses that mediate rapid behavioral responses in fish, electrical synapses are also used broadly in the mammalian brain. For example, they serve to synchronize ensembles of cortical neurons in the cortex and are important for memory consolidation [3–5]. It is intriguing to consider that the neurological circuit defects that characterize ASD could have a basis in defective electrical synaptogenesis. Indeed, it has been suggested that disruption of Cx36-dependent synchronization within the inferior olive contributes to autism by impairing cognitive processing speed [40]. Thus, delineating the biochemical and cell biological role of Nbea in electrical synapse formation may provide critical insight into an underappreciated aspect of this disorder.

Experimental Procedures

Fish, Lines, and Maintenance

All animals were raised at the Fred Hutchinson Cancer Research Center, and animal care and experiments were approved by the Institutional Animal Care and Use Committee. *nbea*^{fh364} was isolated from an early-pressure, gynogenetic diploid screen [20] using ENU as a mutagen. Mutants were maintained in the *M/CoLo:*GFP (*Et*(*Tol-056:GFP*)) background [18]. *nbea*^{fh392} and *nbea*^{fh380} were generated using TALENs [22] targeting the 1st or 21st exon of *nbea*, and stable lines were Sanger sequenced to verify deletions. See Supplemental Experimental Procedures for further details.

RNA-Seq-Based Mutant Mapping

Embryos in the F3 generation were collected at 3 dpf from known *dis4* heterozygous animals and anesthetized with MESAB (Sigma, A5040), and the posterior portion was removed and fixed for phenotypic analysis via immunohistochemistry (see below); the anterior portion was placed in TRIzol (Life Technologies, 15596-026), homogenized, and frozen to preserve RNA for sequencing. After phenotypic identification, mutant (−/−) and wild-type (+/+ and +/−) sibling RNA was pooled separately from 80 embryos each. Total RNA was extracted from each pool, and cDNA libraries were created using standard Illumina TruSeq protocols. Each library was individually bar coded, allowing for identification after multiplexed sequencing on an Illumina HiSeq 2000 machine. There were ~60 million reads per pool, and these were aligned to the zebrafish genome (Zv9.63) using TopHat/Bowtie, an intron- and splice-aware aligner [41]. SNPs were identified using the SAMtools mpileup and bcftools variant caller [42]. Custom R scripts were used to identify high-quality "mapping" SNPs in the wild-type pool; these positions were then assessed in the mutant pool for their frequency. The average allele frequency, using a sliding window of 50 neighboring loci, was plotted across the genome, and linkage was identified as the region of highest average frequency. Within the linked region, candidate mutations causing nonsense or missense changes, or those affecting gene expression levels, were identified using a combination of custom R scripts and existing software (Variant Effect Predictor [43]; Cuffflinks [41]). Details can be found at www.rnamapper.org [21].

Immunohistochemistry

Embryos were fixed and stained using standard procedures. Details on antibodies can be found in the Supplemental Experimental Procedures.

Neurobiotin Retrograde Labeling

Anesthetized 5 dpf embryos were mounted in 1% agar, and a caudal transsection through the dorsal half of the embryo was made with an insect pin at somite 20–25. A second insect pin loaded with 5% Neurobiotin (Nb) solution was quickly applied to the incision. Animals were unmounted from the agar and allowed to rest for 3 hr while anesthetized to allow Nb to pass from M into CoLo. Animals were then fixed in 4% paraformaldehyde for 2 hr and processed for immunohistochemistry. CoLo axons project posteriorly for a maximum of two segments; therefore, measurements of Nb in CoLo were analyzed at least three segments away from the lesion site.

Laser Ablation

M, CoLo, or other control GFP-labeled neurons were ablated at the earliest time each was detectable using a MicroPoint nitrogen laser. Successful ablation was determined by the immediate loss of all GFP fluorescence within the cell body and stereotypical necrotic appearance of the nucleus, and by later absence of the neuron when imaged for experiments.

Cell Transplantation

Cell transplantation was performed using standard techniques [33], and animals were genotyped to confirm transplant categories.

Imaging and Data Analysis

All images were collected on a Zeiss LSM 700 confocal microscope using 405, 488, 555, and 639 laser lines, with each line's data being collected sequentially using standard preprogrammed filters for the appropriate

Alexa dyes. All z stacks used 1 μm steps. Images were processed and analyzed using Zeiss ZEN and Fiji [44] software. Within each experiment, all animals were stained together with the same antibody mix and processed at the same time, and all confocal settings (gain, offset, objective, zoom) were identical. For quantitating fluorescence intensity, synapses were defined as the region of contact between the neurons of interest (M/CoLo for electrical synapse, CoLo/CoLo for the glycinergic synapse). A standard region of interest (ROI) surrounding each synapse was drawn, and the mean fluorescence intensity was measured across at least 4 μm in the z direction with the highest value being recorded. For Nb backfills, fluorescence intensity was measured using a standard ROI encompassing the entire M or CoLo cell body. Dendrite complexity was assessed by first tracing dendrites using the Fiji plugin Simple Neurite Tracer [45]. Dendrite statistics were extracted manually or using the Simple Neurite Tracer's built in algorithms. Statistics were computed using GraphPad Prism software. Figure images were created using Adobe Photoshop and Adobe Illustrator. BitPlane Imaris was used for the digital cross-sections in Figures 7 and S3. In these images only, a mask was created using the GFP channel, and any signal outside the mask was removed; this created a clear view of the M neurons, their dendritic complexity, and the closely associated synaptic staining. Colors for all figures were modified using the Fiji plugin Image5D.

Behavioral Analysis

Behavioral experiments were performed on 6 dpf larvae and filmed using an IDT M3 high-speed camera capturing 500 frames per second. The apparatus for testing startle was adapted from [18]. After behavioral analysis, animals were genotyped.

Supplemental Information

Supplemental Information includes four figures, five tables, Supplemental Experimental Procedures, and two movies and can be found with this article online at http://dx.doi.org/10.1016/j.cub.2014.10.071.

Author Contributions

A.C.M. and L.H.V. performed experiments, acquired and quantified data, and generated images for publication. A.N.S. created the TALENs directed against *nbea* and generated the mutant animals. A.C.M. and C.B.M. wrote the manuscript. All authors edited the manuscript.

Acknowledgments

We thank Rachel Garcia for superb animal care; Kathryn Helde for many, many hours spent in the fish room helping with the forward genetic screen; the C.B.M. lab for discussions and editing; Lila Solnica-Krezel for ENU-mutagenized male zebrafish; Shin-ichi Higashijima for the *M/CoLo:GFP* line; and the Fred Hutchinson Cancer Research Center's Genomic Resource Center, particularly Jeff Delrow, Andy Marty, Alyssa Dawson, and Ryan Basom, for sequencing library preparation, sequencing, and assistance in data processing. Funding was provided by National Institutes of Health grants R01HD076585 and R21NS076950 to C.B.M. and F32NS074839 and K99NS085035 to A.C.M.

Received: September 29, 2014
Revised: October 27, 2014
Accepted: October 28, 2014
Published: December 4, 2014

References

1. Vaughn, J.E., Barber, R.P., and Sims, T.J. (1988). Dendritic development and preferential growth into synaptogenic fields: a quantitative study of Golgi-impregnated spinal motor neurons. Synapse *2*, 69–78.
2. Shen, K., and Scheiffele, P. (2010). Genetics and cell biology of building specific synaptic connectivity. Annu. Rev. Neurosci. *33*, 473–507.
3. Bloomfield, S.A., and Völgyi, B. (2009). The diverse functional roles and regulation of neuronal gap junctions in the retina. Nat. Rev. Neurosci. *10*, 495–506.
4. Peinado, A., Yuste, R., and Katz, L.C. (1993). Extensive dye coupling between rat neocortical neurons during the period of circuit formation. Neuron *10*, 103–114.
5. Pereda, A.E. (2014). Electrical synapses and their functional interactions with chemical synapses. Nat. Rev. Neurosci. *15*, 250–263.
6. Cullinane, A.R., Schäffer, A.A., and Huizing, M. (2013). The BEACH is hot: a LYST of emerging roles for BEACH-domain containing proteins in human disease. Traffic *14*, 749–766.
7. Nuytens, K., Gantois, I., Stijnen, P., Iscru, E., Laeremans, A., Serneels, L., Van Eylen, L., Liebhaber, S.A., Devriendt, K., Balschun, D., et al. (2013). Haploinsufficiency of the autism candidate gene Neurobeachin induces autism-like behaviors and affects cellular and molecular processes of synaptic plasticity in mice. Neurobiol. Dis. *51*, 144–151.
8. Volders, K., Nuytens, K., and Creemers, J.W.M. (2011). The autism candidate gene Neurobeachin encodes a scaffolding protein implicated in membrane trafficking and signaling. Curr. Mol. Med. *11*, 204–217.
9. Su, Y., Balice-Gordon, R.J., Hess, D.M., Landsman, D.S., Minarcik, J., Golden, J., Hurwitz, I., Liebhaber, S.A., and Cooke, N.E. (2004). Neurobeachin is essential for neuromuscular synaptic transmission. J. Neurosci. *24*, 3627–3636.
10. Wang, X., Herberg, F.W., Laue, M.M., Wullner, C., Hu, B., Petrasch-Parwez, E., and Kilimann, M.W. (2000). Neurobeachin: A protein kinase A-anchoring, beige/Chediak-higashi protein homolog implicated in neuronal membrane traffic. J. Neurosci. *20*, 8551–8565.
11. Nair, R., Lauks, J., Jung, S., Cooke, N.E., de Wit, H., Brose, N., Kilimann, M.W., Verhage, M., and Rhee, J. (2013). Neurobeachin regulates neurotransmitter receptor trafficking to synapses. J. Cell Biol. *200*, 61–80.
12. Medrihan, L., Rohlmann, A., Fairless, R., Andrae, J., Döring, M., Missler, M., Zhang, W., and Kilimann, M.W. (2009). Neurobeachin, a protein implicated in membrane protein traffic and autism, is required for the formation and functioning of central synapses. J. Physiol. *587*, 5095–5106.
13. Niesmann, K., Breuer, D., Brockhaus, J., Born, G., Wolff, I., Reissner, C., Kilimann, M.W., Rohlmann, A., and Missler, M. (2011). Dendritic spine formation and synaptic function require neurobeachin. Nat. Commun. *2*, 557.
14. Korn, H., and Faber, D.S. (2005). The Mauthner cell half a century later: a neurobiological model for decision-making? Neuron *47*, 13–28.
15. Hale, M.E., Ritter, D.A., and Fetcho, J.R. (2001). A confocal study of spinal interneurons in living larval zebrafish. J. Comp. Neurol. *437*, 1–16.
16. Liu, K.S., and Fetcho, J.R. (1999). Laser ablations reveal functional relationships of segmental hindbrain neurons in zebrafish. Neuron *23*, 325–335.
17. Pereda, A., O'Brien, J., Nagy, J.I., Smith, M., Bukauskas, F., Davidson, K.G.V., Kamasawa, N., Yasumura, T., and Rash, J.E. (2003). Short-range functional interaction between connexin35 and neighboring chemical synapses. Cell Commun. Adhes. *10*, 419–423.
18. Satou, C., Kimura, Y., Kohashi, T., Horikawa, K., Takeda, H., Oda, Y., and Higashijima, S. (2009). Functional role of a specialized class of spinal commissural inhibitory neurons during fast escapes in zebrafish. J. Neurosci. *29*, 6780–6793.
19. Rash, J.E., Curti, S., Vanderpool, K.G., Kamasawa, N., Nannapaneni, S., Palacios-Prado, N., Flores, C.E., Yasumura, T., O'Brien, J., Lynn, B.D., et al. (2013). Molecular and functional asymmetry at a vertebrate electrical synapse. Neuron *79*, 957–969.
20. Walker, C., Walsh, G.S., and Moens, C. (2009). Making gynogenetic diploid zebrafish by early pressure. J. Vis. Exp. *30*, 1396.
21. Miller, A.C., Obholzer, N.D., Shah, A.N., Megason, S.G., and Moens, C.B. (2013). RNA-seq-based mapping and candidate identification of mutations from forward genetic screens. Genome Res. *23*, 679–686.
22. Sanjana, N.E., Cong, L., Zhou, Y., Cunniff, M.M., Feng, G., and Zhang, F. (2012). A transcription activator-like effector toolbox for genome engineering. Nat. Protoc. *7*, 171–192.
23. Hawrylycz, M.J., Lein, E.S., Guillozet-Bongaarts, A.L., Shen, E.H., Ng, L., Miller, J.A., van de Lagemaat, L.N., Smith, K.A., Ebbert, A., Riley, Z.L., et al. (2012). An anatomically comprehensive atlas of the adult human brain transcriptome. Nature *489*, 391–399.
24. Thisse, B., Pflumio, S., Fürthauer, M., Loppin, B., Heyer, V., Degrave, A., Woehl, R., Lux, A., Steffan, T., Charbonnier, X.Q. and Thisse, C. (2001). Expression of the zebrafish genome during embryogenesis (NIH R01 RR15402). ZFIN Direct Data Submission. http://zfin.org/ZDB-PUB-010810-1.
25. del Pino, I., Paarmann, I., Karas, M., Kilimann, M.W., and Betz, H. (2011). The trafficking proteins Vacuolar Protein Sorting 35 and Neurobeachin interact with the glycine receptor β-subunit. Biochem. Biophys. Res. Commun. *412*, 435–440.
26. Yamanaka, I., Miki, M., Asakawa, K., Kawakami, K., Oda, Y., and Hirata, H. (2013). Glycinergic transmission and postsynaptic activation of

CaMKII are required for glycine receptor clustering in vivo. Genes Cells *18*, 211–224.
27. Lauks, J., Klemmer, P., Farzana, F., Karupothula, R., Zalm, R., Cooke, N.E., Li, K.W., Smit, A.B., Toonen, R., and Verhage, M. (2012). Synapse associated protein 102 (SAP102) binds the C-terminal part of the scaffolding protein neurobeachin. PLoS ONE *7*, e39420.
28. Flores, C.E., Li, X., Bennett, M.V.L., Nagy, J.I., and Pereda, A.E. (2008). Interaction between connexin35 and zonula occludens-1 and its potential role in the regulation of electrical synapses. Proc. Natl. Acad. Sci. USA *105*, 12545–12550.
29. Tyagarajan, S.K., and Fritschy, J.-M. (2014). Gephyrin: a master regulator of neuronal function? Nat. Rev. Neurosci. *15*, 141–156.
30. O'Malley, D.M., Kao, Y.-H., and Fetcho, J.R. (1996). Imaging the functional organization of zebrafish hindbrain segments during escape behaviors. Neuron *17*, 1145–1155.
31. Kohashi, T., and Oda, Y. (2008). Initiation of Mauthner- or non-Mauthner-mediated fast escape evoked by different modes of sensory input. J. Neurosci. *28*, 10641–10653.
32. Burgess, H.A., and Granato, M. (2007). Sensorimotor gating in larval zebrafish. J. Neurosci. *27*, 4984–4994.
33. Kemp, H.A., Carmany-Rampey, A., and Moens, C. (2009). Generating chimeric zebrafish embryos by transplantation. J. Vis. Exp. *17*, 1394.
34. Kimmel, C.B. (1982). Development of synapses on the Mauthner neuron. Trends Neurosci. *5*, 47–50.
35. Siddiqui, T.J., and Craig, A.M. (2011). Synaptic organizing complexes. Curr. Opin. Neurobiol. *21*, 132–143.
36. Sin, W.C., Haas, K., Ruthazer, E.S., and Cline, H.T. (2002). Dendrite growth increased by visual activity requires NMDA receptor and Rho GTPases. Nature *419*, 475–480.
37. Elias, L.A.B., Wang, D.D., and Kriegstein, A.R. (2007). Gap junction adhesion is necessary for radial migration in the neocortex. Nature *448*, 901–907.
38. Kimmel, C.B., Powell, S.L., and Kimmel, R.J. (1982). Specific reduction of development of the Mauthner neuron lateral dendrite after otic capsule ablation in Brachydanio rerio. Dev. Biol. *91*, 468–473.
39. Krumm, N., O'Roak, B.J., Shendure, J., and Eichler, E.E. (2014). A de novo convergence of autism genetics and molecular neuroscience. Trends Neurosci. *37*, 95–105.
40. Welsh, J.P., Ahn, E.S., and Placantonakis, D.G. (2005). Is autism due to brain desynchronization? Int. J. Dev. Neurosci. *23*, 253–263.
41. Trapnell, C., Roberts, A., Goff, L., Pertea, G., Kim, D., Kelley, D.R., Pimentel, H., Salzberg, S.L., Rinn, J.L., and Pachter, L. (2012). Differential gene and transcript expression analysis of RNA-seq experiments with TopHat and Cufflinks. Nat. Protoc. *7*, 562–578.
42. Li, H., Handsaker, B., Wysoker, A., Fennell, T., Ruan, J., Homer, N., Marth, G., Abecasis, G., and Durbin, R.; 1000 Genome Project Data Processing Subgroup (2009). The Sequence Alignment/Map format and SAMtools. Bioinformatics *25*, 2078–2079.
43. McLaren, W., Pritchard, B., Rios, D., Chen, Y., Flicek, P., and Cunningham, F. (2010). Deriving the consequences of genomic variants with the Ensembl API and SNP Effect Predictor. Bioinformatics *26*, 2069–2070.
44. Schindelin, J., Arganda-Carreras, I., Frise, E., Kaynig, V., Longair, M., Pietzsch, T., Preibisch, S., Rueden, C., Saalfeld, S., Schmid, B., et al. (2012). Fiji: an open-source platform for biological-image analysis. Nat. Methods *9*, 676–682.
45. Longair, M.H.M., Baker, D.A.D., and Armstrong, J.D.J. (2011). Simple Neurite Tracer: open source software for reconstruction, visualization and analysis of neuronal processes. Bioinformatics *27*, 2453–2454.